This manuscript was published as formal in:

International Journal of Biological Macromolecules 2022, 205, 574-586

DOI: 10.1016/j.ijbiomac.2022.02.077

https://doi.org/10.1016/j.ijbiomac.2022.02.077

***Title*:**

Chitosan crosslinking with a vanillin isomer towards self-healing hydrogels with antifungal activity

Manuela-Maria Iftime[1]*, Irina Rosca[1], Andreea-Isabela Sandu[1], Luminita Marin[1]

[1] “Petru Poni” Institute of Macromolecular Chemistry, Grigore Ghica Voda Alley, Iasi, Romania

*ciobanum@icmpp.ro

Abstract

The purpose of the study was to develop new antimicrobial hydrogels from natural resources that may promote wound healing and prevent bacterial skin infection. The new hydrogels were synthesized by crosslinking chitosan with a vanillin isomer, 5-methoxysalicylaldehyde, by a friendly and easy method. To characterize these hydrogels, their structural and morphological properties were explored by FTIR, ^{1}H-NMR, SEM, POM, and TGA. In view of the targeted application, swelling behavior, biodegradability, antimicrobial activity and biocompatibility were investigated *in vitro*. Structural and morphological studies confirmed the formation of new hydrogels *via* the imination reaction concomitant with the supramolecular organization. The hydrogels were highly porous with the average pore diameter around 80 µm, and a swelling rate controlled by the crosslinking density and medium pH. The hydrogels showed a progressive weight loss in the presence of lysozyme up to 35 %, during 21 days of testing. They proved non-cytotoxic effect on normal human dermal fibroblasts using MTS test and powerful antifungal activity against *Candida Albicans*, as determined by disk diffusion assay. All these properties indicate the new hydrogels as a promising option for the treatment of various skin lesions.

Keywords: chitosan, biodegradability, antifungal activity, non-toxicity

1. Introduction

In recent years, there was a growing global demand for new wound dressing materials to the increased resistance of pathogens to last-line antibiotics, which cause serious infections and wound-repair difficulties, leading to the loss of many human lives [1]. The ideal wound dressings should be easy and inexpensive to synthesize, sterile and non-toxic, biodegradable, to have good absorption of wound exudate and good gas permeability, and most importantly to have antimicrobial properties [2]. In this regard, varieties of wound dressing materials have been obtained either based on synthetic or natural polymers and are formulated in various forms such as membranes, films, fibers, topical formulations, transdermal patches, sponges, hydrogels and so on [3-6]. However, even some of these materials are effective in preventing bacterial infection of skin wounds, they suffer from several limitations such as high cost, weak mechanical performance, and difficulty to be removed without lesion damage, or inability to provide a moisture environment for acceleration of the wound healing process [7]. Considering these limitations, the development of more advanced wound dressings that are cost-effective is still a goal for researchers in clinical application [8].

Hydrogels are made up of a three-dimensional network that can absorb large amount of water and have a number of common physical properties with living tissues such as softness, elasticity and low interfacial tension, which are favorable for good compatibility and improve the healing process [9, 10]. Chitosan is known as the most important natural originating polymer that can be used to produce wound dressings due to its various versatile properties such as good biodegradability, biocompatibility, antibacterial and hemostatic effect, non-toxicity, bio-adhesivity and availability of functional groups for its modification [11-13]. In terms of wound treatment, chitosan-based hydrogels are considered as ideal materials which possess all the above properties [14, 15]. Compared to traditional wound dressings like cotton, wool or gauze, they are easier to peel off and degrade spontaneously, avoiding the discomfort and secondary trauma of dressing replacement [16]. Moreover, their porous structure and a suitable swelling ratio allow the oxygen permeation and exudate drainage while keeping a moist environment, which is beneficial for wound healing [17, 18] The main disadvantages of chitosan hydrogels for wound management are their drying up if they are not covered, difficulty to secure them, and poor mechanical stability in swollen state [19]. A promising approach to overcome these disadvantages can be the crosslinking of chitosan with natural monoaldehydes, which determine the enhancing of physical, chemical and mechanical properties (mechanical and thermal stability, swelling capacity, biodegradability and biocompatibility). Over last years, our group demonstrated that chitosan crosslinking with monoadehydes, *via* formation of imine units and their self-assembling into clusters, is a simple method towards hydrogels with properties tailored by a proper choice of the aldehyde [20-27].

Taking into account these data, this paper reports the synthesis of chitosan hydrogels with inherent antimicrobial properties by crosslinking with a natural monoaldehyde, 5-methoxysalicylaldehyde (A). It should be highlighted that this aldehyde is one of the isomers of vanillin, a naturally occurring derivate of benzaldehyde, which has already demonstrated significance in food, cosmetics, chemical and pharmaceutical industries [28]. Its choice was done targeting biocompatible hydrogels with antimicrobial properties capable to promote wound healing and prevent the bacterial skin infections. Moreover, compared to traditional wound dressings, these hydrogels are expected to be biodegradable, avoiding by this the traumatic debridement. The hydrogels were characterized in relationship with the envisaged applications, their properties such as swelling in media with different pH, biodegradation, biocompatibility, self-healing and antimicrobial activity being investigated. They showed porous morphology and good swelling ability which can assure the exudate drainage maintaining a moist environment useful to promote wound healing. They were thermally stable,

biodegradable and pH-sensitive, and presented antimicrobial performance against *Candida albicans*, self-healing behavior and good biocompatibility, indicating great potential for use in the treatment of skin lesions. To the best of our knowledge, this is the first study which reports the synthesis and performances of chitosan hydrogels cross-linked with the natural monoaldehyde, 5-methoxysalicylaldehyde.

3.1.2. Material and methods

2.1. Materials

Low molecular weight chitosan, 5-methoxysalicylaldehyde of 98% purity, (**A**), ethanol (99.8%) and glacial acetic acid (99%) were purchased from Aldrich Co. (USA) and used as received. The average viscometric molecular weight of chitosan (M_v) was calculated by viscosimetry (M_v=198kDa) and the deacetylation degree (DA=82%) was calculated by ^{1}H-NMR (Fig. S1 and Fig. S2) [13]. The total of the free amino groups of chitosan was calculated considering the DA. Acetate buffer solution of pH=5.5 and phosphate buffer (PBS) of pH=7.4 and 8.5 were prepared in our laboratory, as already reported [20-23]. Bidistilled and ultrapure water were obtained in our laboratory, too.

2.2. Synthesis of 5-methoxysalicyl-imine-chitosan hydrogels (Hx)

The synthesis was carried out by acid condensation reaction of chitosan with 5-methoxysalicylaldehyde (**A**), adapting a procedure reported for other chitosan/aldehyde systems [20]. 0.480 g chitosan (corresponding to $2.32*10^{-3}$ mmol glucosamine repeating units) were dissolved in 24 mL acidic water (0.7% acetic acid solution: 168 μL of acetic acid in 24 mL of water) under vigorous magnetic stirring (750 rpm). Further, the chitosan solution was heated at 55^{o}C, and a 2% solution of 5-methoxysalicylaldehyde (**A**) in ethanol was slowly dropped into it and the reaction mixture was maintained until hydrogelation occurred. In order to reach hydrogels with different crosslinking degrees, the 5-methoxysalicylaldehyde (**A**) amount was varied to attain molar ratios of the NH_2 and CHO functional groups from 1/1 up to 6/1 (Table 1). The hydrogelation time depended on the NH_2/CHO molar ratio, varying from 1 minute to 7 days as the aldehyde amount decreased (Table 1). In order to remove the ethanol, the vials were kept uncovered up to the initial volume of chitosan solution was reached. The as obtained hydrogels (noted ***Hx***, where **x** is the molar ratio of the NH_2/CHO functional groups) appeared as transparent, deep yellow semisolid materials, with smooth texture (Scheme 1). Their corresponding solid materials (xerogels) were prepared by hydrogels' lyophilization. The xerogels weight was similar with that of the initial reagents, indicating no mass loss during lyophilization, and implicit the total reaction of the reagents.

Tabel 1. The reaction parameters and codes of the studied hydrogels (***Hx***)

Code	**H1**	**H1.5**	**H2**	**H3**	**H4**	**H5**	**H6**
NH_2/CH=O	1/1	1.5/1	2/1	3/1	4/1	5/1	6/1
Chitosan (mg/mmol)	480/2.32*10^{-3}						
A (mg/mmol)	353/ 2.32x10^{-3}	235/ 1.54x10^{-3}	177/ 1.16x10^{-3}	117 7.7x10^{-4}	88/ 5.8x10^{-4}	71/ 4.61x10^{-4}	59/ 3.9x10^{-4}
Water (mL)	24						
Ethanol (mL)	17.66	11.77	8.83	5.88	4.42	3.53	2.94
Acetic acid (ml)	0.168						
Gelation time	1min	2 min	5 min	30 min	1day	2days	7days
Xerogel (g)	0.833	0.715	0.657	0.597	0.568	0.551	0.539

A: 5-methoxysalicylaldehyde;

2.3. Characterization

2.3.1. The dry state of the hydrogels (xerogels) was obtained by freezing in liquid nitrogen and further lyophilisation using Labconco Free Zone Freeze Dry System equipment, at -52 ºC and 1.510 mbar for 48 hours.

2.3.2. ***The ^{1}H-NMR spectra* (*NMR*)** were achieved on a Bruker Advance DRX 400 MHz Spectrometer equipped with a 5 mm QNP direct detection probe and z-gradients. For NMR measurements, the hydrogels were prepared directly into NMR tubes using deuterated water. The chemical shifts were reported as δ values (ppm) relative to the residual peak of deuterated water.

2.3.3. Fourier transformed infrared spectroscopy (FTIR). ATR-FTIR spectra were registered with a Bruker Vertex 70 Ettlingen FTIR spectrometer, on pellets obtained by pressing 20 mg of xerogels into a hydraulic press at 2 N/m^2. The spectra were recorded in the 600–4000 cm^{-1} spectral range, with 32 scans at 4 cm^{-1} resolution. The presence of the imine linkage was confirmed by deconvolution of the 1690-1615 cm^{-1} region of the FTIR spectra. The overlapped peak positions from this region were determined with the second derivative. After that, the stretching vibration regions were deconvoluted by a curve-fitting mode, and the areas were calculated with a 50% Lorentzian and 50% Gaussian function. The OPUS 6.5 software and OriginProBit9 were used to perform the curve-fitting analysis [29].

2.3.4. To gain an insight on the hydrogel morphology, images of the corresponding xerogels were acquired with a field emission ***Scanning Electron Microscope (SEM)*** EDAX – Quanta 200 at accelerated electron energy of 20KeV.

2.3.5. ***Polarized light microscopy*** observations were performed with a Zeiss Axio Imager.A2m, camera Axiocam 208cc, Carl Zeiss AG, (Oberkochen, Germany) microscope, on thin slices of hydrogels.

2.3.6. ***X-ray diffraction investigation*** was done on a Rigaku Miniflex 600 diffractometer by CuKα-emission in the angular range 2–40º (2θ) using a scanning step of 0.0025º and a recording rate of 1º/min.

2.3.7. The ***thermogravimetric analysis (TGA)*** was performed on xerogel samples with a Discovery TGA 5500 equipment, under nitrogen atmosphere, at the constant heating rate of 10°C/min from 30 to 600ºC. The amount of each sample was approx. 7 mg. The temperature corresponding to 10% (T_{10}) weight loss, and the temperature of maximum decomposition rate, corresponding to the peak in DTG curve (T_{dec}), have been taken as characteristic conditions when discussing the thermal stability.

2.3.8. The UV-Vis spectra were recorded on an ***UV-visible spectrophotometer*** (Perkin Elmer, Lambda 10). The *in vitro* aldehyde release was investigated by monitoring the released aldehyde by quantitative absorption spectroscopy, as follows. 120 mg hydrogel was immersed into a vial containing 10 mL of ultrapure water, at 37ºC. At fixed intervals, 2 mL aliquots were withdrawn and replaced with 2 mL fresh ultrapure water. The supernatant samples were collected and subjected to aldehyde absorbance measurements by UV-vis spectroscopy, recording the specific absorption band at 258.87 nm. Further, the absorbance values were fitted on a predetermined calibration curve to give the aldehyde concentrations. The cumulative release of **A** was calculated with the equation: % **A** = $[(10C_n + 2\Sigma C_{n-1})/m_o]$ x 100, and was plotted versus time to give the release kinetic, where C_n and C_{n-1} represent the concentrations of the aldehyde in the supernatant after n and n-1 withdrawing steps, respectively, and m_o, correspond to the aldehyde's content.

2.3.9. ***Swelling behavior and stability of the hydrogels in media with different pH***

The swelling ability of the hydrogels was investigated on the samples which showed the most important properties (***H1.5***, ***H2*** and ***H3***) in distilled water and buffer solution of different pH = 5.5, 7.4 and 8.5, at 37ºC [4]. Certain amounts around 100 mg of hydrogels were immersed into vials containing 10 mL of swelling media, and the samples were taken off and weighted at known time periods until they reached a constant mass. After that, they were washed with

ultrapure water and dried by lyophilisation to calculate their weight loss. The percentage of swelling ratio (SR) of the hydrogels was calculated using the equation (1):

$$SR = (W_s - W_d)/W_d \times 100 \quad \textbf{(1)}$$

where W_s and W_d are the weights of the swollen and the initial hydrogels, respectively. The weight loss percent was calculated with equation (2):

$$\text{Weight loss } \% = W_0 - W_t/W_0 \times 100 \quad \textbf{(2)}$$

where W_0 is the initial weight of the freeze-dried hydrogels; W_t is the weight of the freeze-dried hydrogel at the end of swelling experiment (2 days). To know exactly the initial weight of the freeze-dried hydrogels, the same amount of the hydrogels used in the swelling study was lyophilized during 24h.

The hydrolytic stability of the hydrogels was visually monitored by immersing pieces of hydrogels of 100 mg in the same media used in the swelling study, over 2 days and 3 months [30-32].

2.3.10. In vitro enzymatic biodegradation of the hydrogels

The hydrogels were incubated in solution of lysozyme in PBS (pH=8.5), 10mg/L (400000U/L) at 37 ºC for 21 days. The incubation medium was refreshed at every three days in order to maintain the enzymatic activity. The samples were carefully taken out at predetermined time intervals of 1, 2, 3, 4, 7, 14 and 21 days, washed with ultrapure water, and lyophilized [33]. The hydrogels' biodegradation was assessed by calculating the mass loss using the equation (3):

$$\text{Weight loss} = (W_0 - W_t)/W_0 \times 100 \quad \textbf{(3)}$$

where W_0 is the initial weight of the freeze-dried hydrogels and W_t is the weight of the freeze-dried hydrogel at the time t.

2.3.11. *Cytotoxicity of chitosan hydrogels*

Cell culture: Normal human dermal fibroblasts (NHDF, PromoCell, Heidelberg, Germany) were grown in alpha-MEM medium (Lonza, Basel, Switzerland) supplemented with 10% fetal bovine serum (FBS, Gibco, Thermo Fisher Scientific, Waltham, MA USA) and 1% Penicillin-Streptomycin-Amphotericin B mixture (Lonza, Basel, Switzerland) in humidified atmosphere with 5% CO_2, at 37 °C.

Cytotoxicity of chitosan hydrogels: Cytotoxicity of ***Hx*** hydrogels was assessed by MTS assay using the CellTiter 96® AQueous One Solution Cell Proliferation Assay (Promega, Madison, WI USA), according to the manufacturer instructions and direct contact procedure adapted from ISO 10993-5:2009(E) [34]. For this purpose, cells were seeded at a density of

5×10^3 cells/mL into 96-well tissue culture-treated plates in 100 µL culture medium/well and allowed to adhere for 24h. Cells were then incubated for another 24 hours with 200 µl culture medium and 10 (± 0.01) mg of each hydrogel sample (3mm diameter). Before incubating, the hydrogel samples were immersed in 70% ethanol, washed with ultrapure water, with culture medium and exposed to UV light (253.7 nm) for 30 minutes. Control cells were incubated only with culture medium. The next day, the medium in the wells containing the tested material was replaced with 100 µl fresh medium and MTS reagent (20 µL) was added 1-3 hours prior to absorbance readings at 490 nm on a FLUOstar® Omega microplate reader (BMG LABTECH, Ortenberg, Germany). Experiments were done in triplicate and treated cell viability was expressed as percentage of control cells' viability. Graphical data were expressed as means ± standard error of the mean. Statistical analysis was performed using GraphPad Prism 7 with One-way Anova using Kruskal-Wallis test with Dunn's multiple comparisons test. The differences were considered statistically different when $p<0.05$.

Cell morphology: To confirm the MTS assay, morphology of the cells exposed to the chitosan hydrogel samples was analyzed by optical microscopy. The hydrogel samples were cut into 1 cm diameter pieces, immersed in 70% ethanol, washed with ultrapure water, with culture medium and sterilized by exposure to UV light (253.7 nm) for 30 minutes. The samples were placed into a 24-well tissue culture treated plate and NHDF cells were seeded onto sterilized hydrogels at a density of $1x10^5$ cells/mL in 1 mL culture medium/well. Cells were then incubated for 24 hours. Control cells were incubated only with culture medium. After 24 hours, brightfield images were acquired with a Leica DMI 3000B inverted microscope (Wetzlar, Germany).

2.3.12. *Antimicrobial activity*

The antimicrobial activity screening of the hydrogels was determined by disk diffusion assay [35] against three bacterial strains: *Staphylococcus aureus* ATCC25923, *Escherichia coli* ATCC25922 and *Enterococcus faecalis* ATCC 29212, two yeast strains *Candida albicans* ATCC10231 and *Candida glabrata* ATCC 2001, and three fungal strains: *Penicillium chrysogenum* ATCC10106, *Cladosporium cladosporioides* ATCC16022 and *Aspergillus brasiliensis* ATCC9642. All microorganisms were stored at -80 °C in 20-40% glycerol. The bacterial strains were refreshed on tryptic soy agar (TSA) at 37 °C for 24 hours. The yeast strains were refreshed on Sabouraud dextrose agar (SDA) and the fungal strains were refreshed on potato dextrose agar (PDA) for *C. cladosporioides* and *A.brasiliensis* and malt extract agar (MEA) for *P. chrysogenum* at 25°C for 72 hours. Microbial suspensions were prepared with these cultures in sterile solution to obtain turbidity optically comparable to that of 0.5

McFarland standards. Volumes of 0.2 ml from each inoculum were spread on the Petri dishes. The sterilized paper disks were placed on the plates and an aliquot (50 µl) of the samples was added. To evaluate the antimicrobial properties, the growth inhibition was measured under standard conditions after 24 of incubation at 37°C for the bacterial strains and the yeast strains and after 72 hours at 25ºC for the fungal strains. All tests were carried out in triplicate to verify the results. After incubation, the diameters of inhibition zones were measured by using Image J software and were expressed as the mean ± standard deviation (SD). Statistical analysis was performed XLSTAT software [36].

Statistics

All experiments were done in triplicate and the data were considered as the mean ± standard deviation (SD).

3. RESULTS AND DISCUSSION

A series of six hydrogels was prepared by acid condensation reaction of chitosan with 5-methoxysalicylaldehyde (***A***), varying the molar ratio between glucosamine units of chitosan and aldehyde groups (Table 1). The schematic representation of their synthesis was shown in Scheme 1. As previously demonstrated for crosslinking of chitosan with monoaldehydes, the hydrogelation was expected to take place due to the formation of imine linkages on the chitosan chains, and the self-ordering of these new formed imine units into clusters, playing the role of crosslinking nodes for chitosan chains [20-27]. This hydrogelation pattern was confirmed by structural and supramolecular investigations by ^{1}H-NMR, FTIR, WRXD, and POM, which were performed on the hydrogels and their corresponding xerogels and analyzed in details.

Scheme 1. Schematic representation for the hydrogels' obtaining (***Hx)***

3.1. Structural characterization

The ***^{1}H-NMR spectra*** of hydrogels (***H1.5-H5*)** revealed the formation of imine linkage by the occurrence of the chemical shift of imine proton as a single band at 8.39 ppm [20]. During the first 3 hours after hydrogelation, the aldehyde proton was also seen at 9.82 ppm, but it almost completely disappeared after 7 days, indicating the progressive conversion of aldehyde into imine units (Fig.1, Fig. S3). Compared to other hydrogels prepared from chitosan and monoaldehydes [21, 23, 24, 33] the high imination yield was attributed to the stabilization of the imine linkages by an intramolecular H-bond with the neighbor proton from hydroxyl group, by a "clip-effect" [22, 37, 38]. The chemical shifts of the other protons from 5-methoxysalicylaldehyde and chitosan were also present in the spectra.

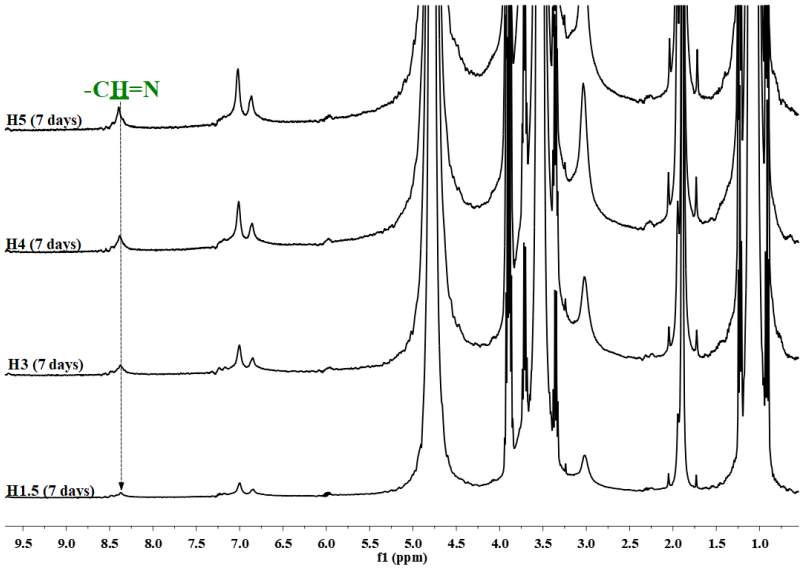

a)

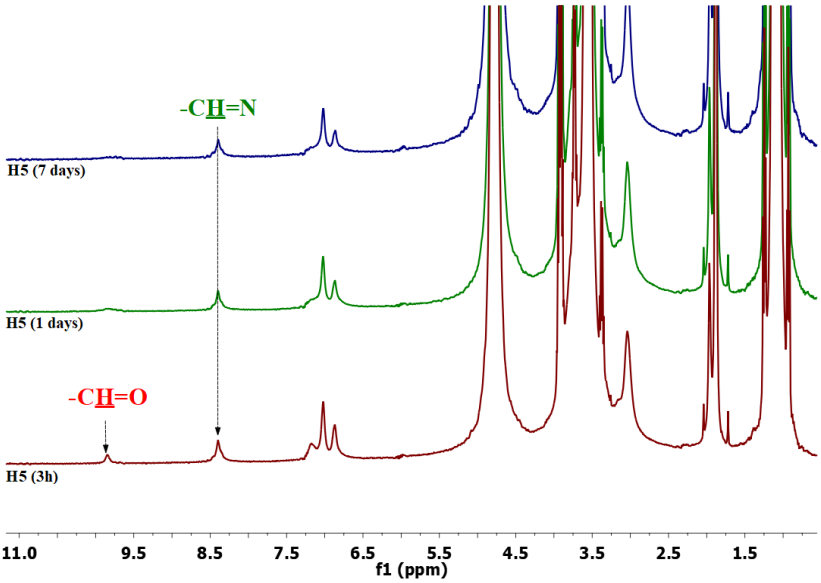

b)

***Fig.** 1*. (a) NMR spectra of representative hydrogels recorded after 7 days since hydrogelation; (b) NMR spectra of the sample $\boldsymbol{H_5}$ recorded at different moments over 7 days

FTIR spectra of the corresponding xerogels showed modifications compared to those of precursors, i.e. chitosan and 5-methoxysalicylaldehyde, consistent with the formation of the imine linkages (Fig.2, Fig.S4). Thus, the broad band characteristic for the vibration of amide group in chitosan (around 1639 cm^{-1}) transformed into a sharp band with maximum at 1637 cm^{-1} with a shoulder to higher wavenumbers, the most probably resulting from the overlapping of imine and amide bands (Fig. 2a). The deconvolution of 1690-1615 cm^{-1} spectral domain, indeed revealed the appearance of a new band at 1633 cm^{-1}, characteristic for the vibration of imine linkage stabilized by a "clip-effect" (Fig. 2b, 2c) [20]. No characteristic band for the vibration of aldehyde group of 5-methoxysalicylaldehyde (1661 cm^{-1}) was detected confirming its total consumption. Comparing the xerogels' spectra, a diminishing of the intensity of the imine absorption band was evident along the decreasing the ***A*** reagent (Fig.S4) [39]. Other absorption bands characteristic to the aliphatic stretching vibration originating from chitosan (2924 and 2876 cm^{-1}) and the double bond stretching vibrations originating from 5-methoxysalicylaldehyde (1591 and 1486 cm^{-1}) were also present [26]. Spectral modifications were also observed in the domain characteristic for the vibrations of amine and hydroxyl groups in chitosan and their *intra*- and *inter*- molecular H-bonds. While chitosan showed a broad band with two maxima at 3401 and 3283 cm^{-1}, attributed to the symmetric and asymmetric vibration of the amine units, the xerogels showed a maximum around 3459 cm^{-1}, possible correlated with the new intra-molecular H-bonds between imine nitrogen and H atom of the hydroxyl groups [20, 40].

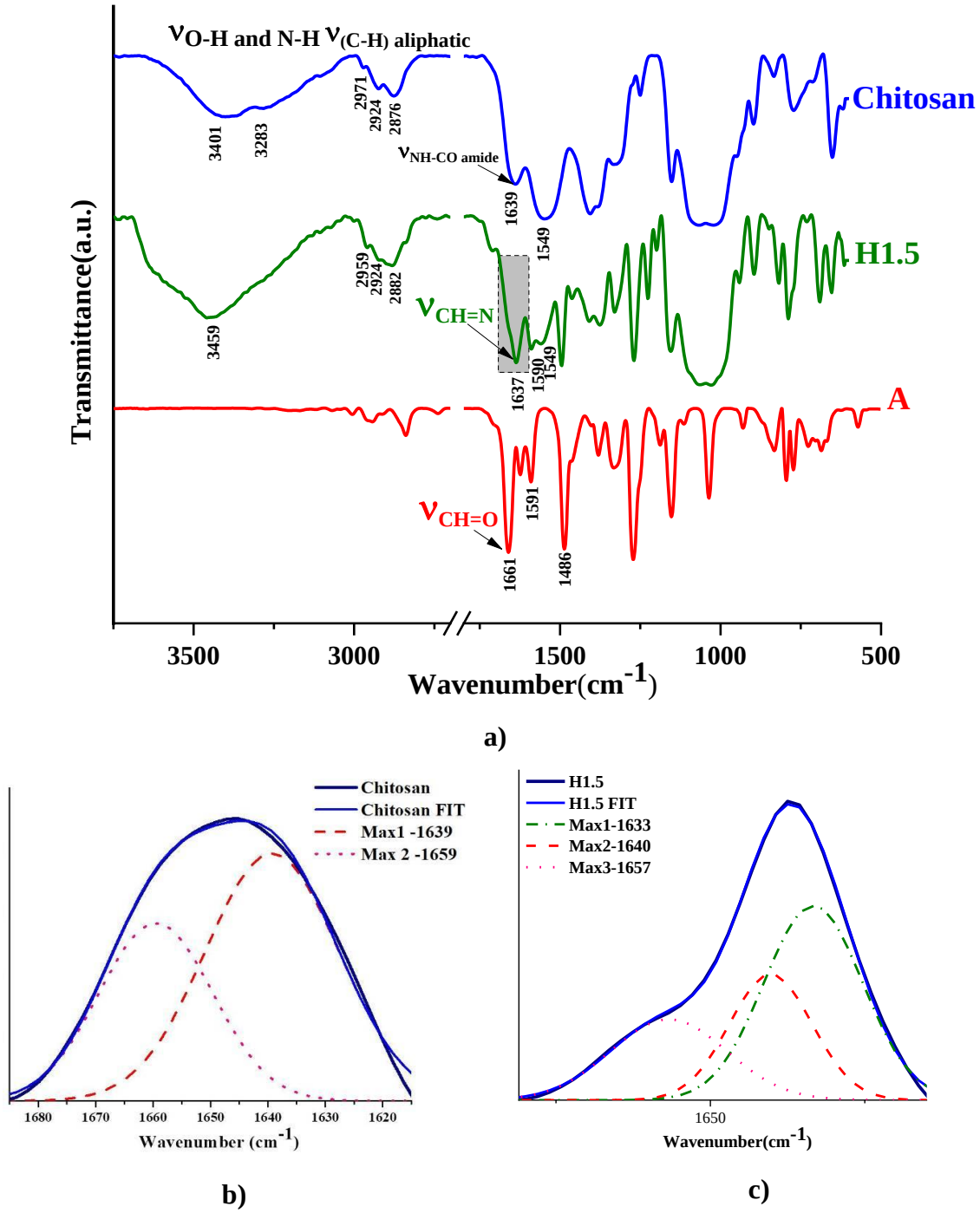

Fig.2. a) The FTIR spectra of the ***A***, ***H1.5*** and ***chitosan*** and *b)* deconvolution of the 1690-1615 cm^{-1} spectral domain for chitosan and ***H1.5***.

3.2 Supramolecular characterization

The preliminary investigation of the supramolecular ordering of the imine units into clusters was done by observing the hydrogels under polarized light. As can be seen in Fig.3a,b, the hydrogels showed strong birefringence with a banded texture, characteristic for layered architectures of the ordered clusters [20, 22]. The hypothesis of the ordered clusters was also

supported by the yellowish luminescence of the hydrogels when illuminated with an UV-lamp, attributable to the emission of new fluorophores formed *via* the space conjugation of the imine subfluorophores (Fig.3c, d) [41].

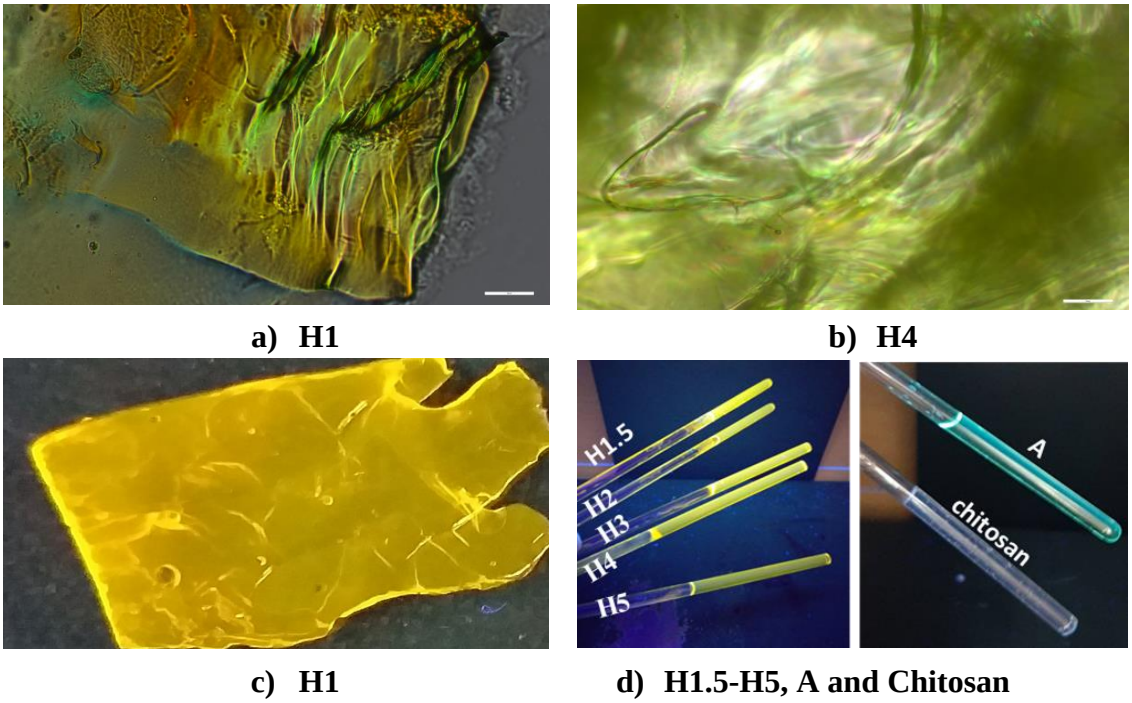

a) H1 **b) H4**

c) H1 **d) H1.5-H5, A and Chitosan**

Fig. 3. a,b) POM images of representative hydrogels (scale: 50 μm) and c,d) hydrogels and chitosan and **A** solutions illuminated with an UV lamp

Further, in order to evidence the self-assembling of the newly formed imine units, wide angle X-ray diffraction on xerogels was performed. As can be seen in Fig. 4 the chitosan diffractogram suffered major modification after hydrogelation with 5-methoxysalicylaldehyde, mainly consisting in the occurrence of a sharp reflection band at 5.9 ^{o}, characteristic to a layer periodicity [20-24]. The corresponding inter-layer distance of 14.99-14.04 Å was in good agreement with the inter-layer spacing into a layered architecture with partial overlapping of the imine units of adjacent layers [42]. Besides, the broad reflection of chitosan at 21.8 ^{o} shifted to lower angle at 20.7^{o} and a new reflection appeared at 13^{o}, consistent with inter-chain (4.4 Å) and inter-molecular (6.8 Å) distances into the 3D ordered clusters (Table S1) [20-24]. Regarding the WXRD diffractograms of different xerogels, it can be observed that the intensity of the inter-layer reflection decreased along the imination degree, in agreement with the decreasing of the clusters' density (Table S1).

All these data confirmed that the formation of the imine units and their self-ordering into clusters are the driving forces of the hydrogelation process of chitosan with 5-methoxysalicylaldehyde.

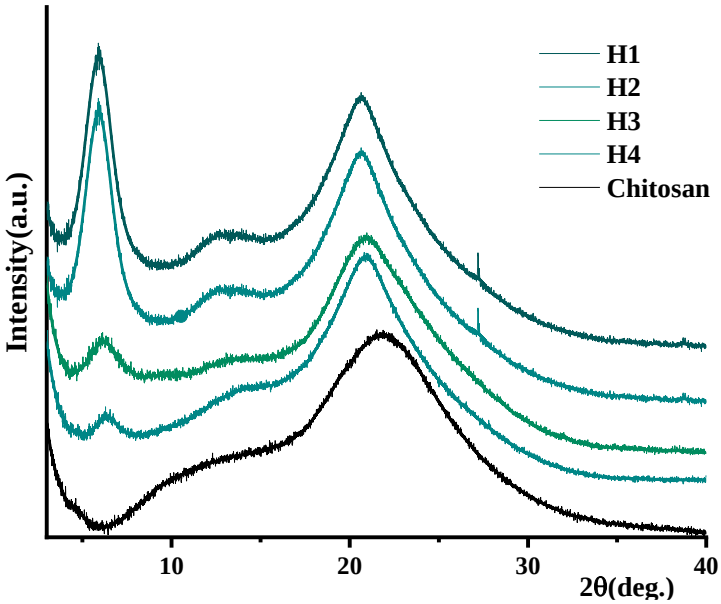

Fig. 4. WXRD of the chitosan and representative xerogels

3.3. Thermogravimetric Analysis (TGA)

Thermal analysis of the xerogels and their precursors revealed interesting aspects related to the physicochemical properties of the hydrogels. First, the rapid mass loss characteristic to the aldehyde volatilization [43] was not detected in the ATG/DTG curves of the xerogels (Fig.5a,b), confirming its chemical bonding to chitosan chains by imination, as ^{1}H-NMR and FTIR spectra indicated. TGA curves showed an evident improvement of the thermal stability as the imination degree increased, i.e. the T_{10} (corresponding to 10% weight loss) recorded at 110^{o}C for chitosan, progressively shifted from 112^{o}C (***H5***) to 273^{o}C (***H1***) for xerogels. The improving of thermal stability was attributed to the effect of crosslinking by imination and formation of ordered clusters. The ***H1*** showed the highest thermal stability, according to a dense network determined by the almost total imination of the amine groups of chitosan. A deeper insight gained from the DTG curves (Fig. 5b) show that the first degradation stage corresponding to the evaporation of adsorbed water occurred at lower temperatures for xerogels compared to pristine chitosan, in agreement with the imination occurrence which disturbed the H-bonds of water to amine units [44]. The most important thermogravimetric characteristics of the representative xerogels, obtained from the thermograms are listed in Table S2.

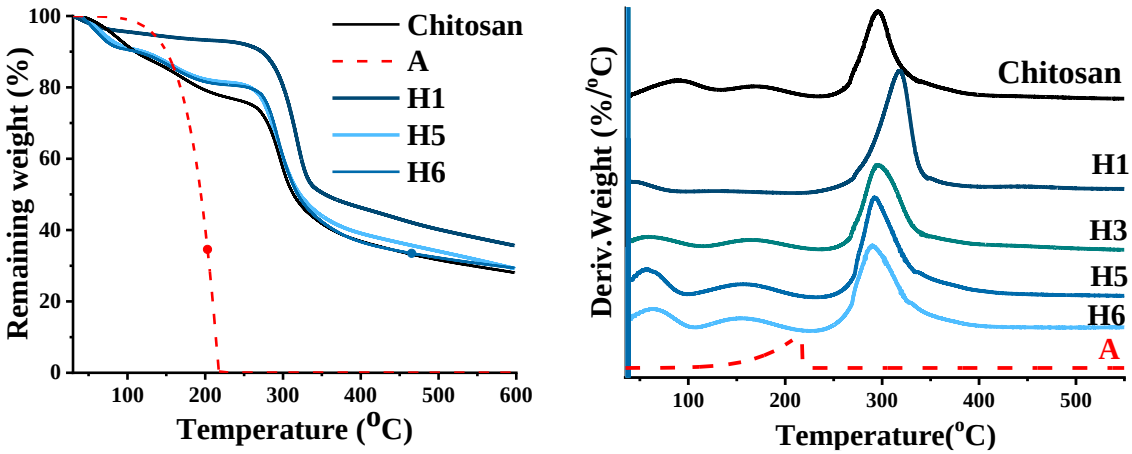

***Fig. 5. a*)** The thermograms and **b**) DTG curves of chitosan, **A** and some representative freeze-dried hydrogels

3.4. Morphology of the 5-methoxysalicyl-imine-chitosan hydrogels

SEM images acquired on freeze-dried hydrogels clearly showed the presence of large quantities of interconnected pores with irregular shape indicating a porous or fibrous structure, depending on the aldehyde content [45]. As can be seen in Figure 6 and Figure S5, the hydrogel with lowest crosslinking degree (***H6***) presented a fibers network, those with intermediate crosslinking degree displayed irregular pores and fibers connected together (***H3***, ***H4*** and ***H5***), and those with higher crosslinking degree (***H1, H1.5*** and ***H2***) showed interconnected pores with diameters around 85-100 µm. It appears that the hydrogel morphology can be tuned by a proper choice of the amount aldehyde crosslinker.

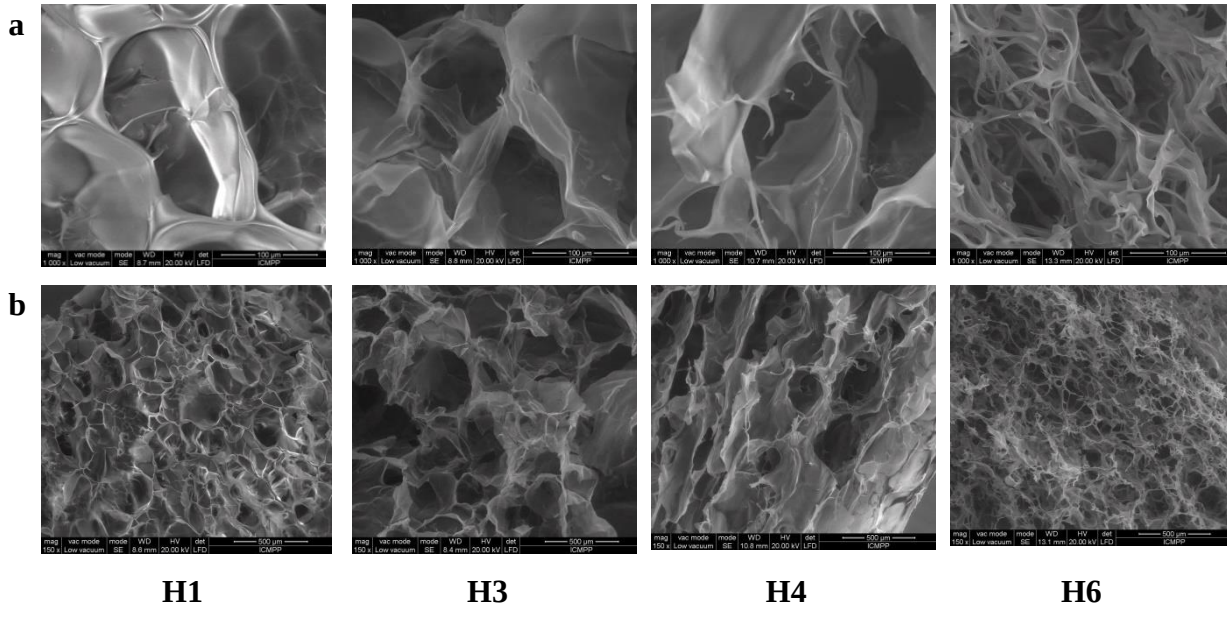

Fig.6. SEM images of freeze-dried hydrogels at different magnifications: a) 1000x; b) 150x

3.5. Cytotoxicity of chitosan hydrogels (MTS assay)

The main condition for *in vivo* application of materials is their biocompatibility. The studied hydrogels were obtained from natural originating reagents, which should account for non-toxicity, biodegradation and biocompatibility, assuring a good acceptance into tissues [46]. In this view, the response of NHDF cells at the contact with the studied hydrogels and pristine reagents was investigated, according to ISO 10993-5:2009(E) test for medical devices that recommend the use of materials for biomedical purposes for cell viability higher than 70% [34]. As can be seen in figure 7, the ***H1.5***, ***H2*** and ***H3*** proved suitable biocompatibility for *in vivo* applications, while those with higher or lower crosslinking degrees showed higher cytotoxicity than accepted for medical devices.

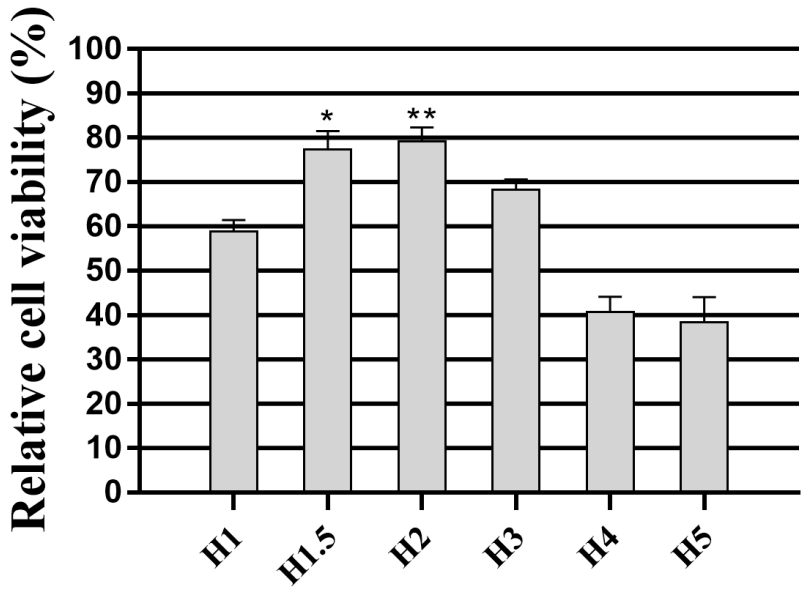

Fig.7. Cell viability of normal human dermal fibroblasts (NHDF) after 24 hours exposure to hydrogels, compared to untreated cells. The results are presented as mean value ± the standard error of the mean (SEM), n = 5; * $p<0.05$ (H1.5 vs. H4, H1.5 vs. H5) and ** $p<0.01$ (H2 vs. H4, H2 vs. H5).

Cell Morphology

Brightfield images were acquired only for those samples that indicated higher viability. The morphology of cells incubated with ***H1.5*** and ***H2*** was normal, NHDF cells keeping their characteristic elongated form (Figure 8). Some of the cells incubated with ***H3*** have a rounded shape, which indicates their partial detachment from the substrate, this being in agreement with the result of the MTS test. Finally, the increased viability of cells incubated in the presence of hydrogels indicates their usefulness in wound healing applications.

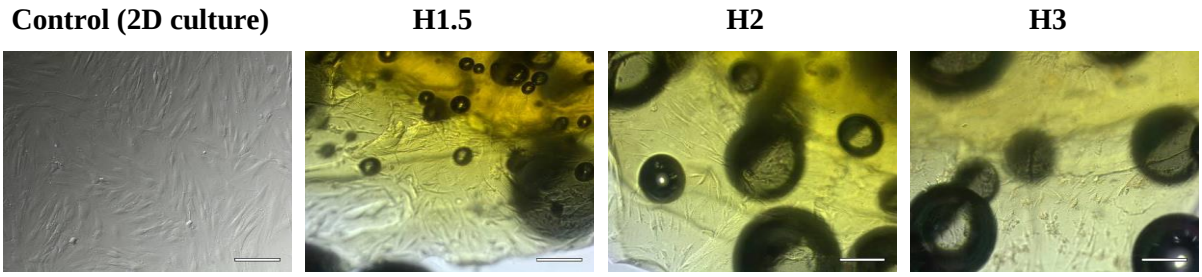

Fig.8. Brightfield images indicating cell morphology in control and in culture-treated plates. The scale represents 200 μm (bubbles in the treated plates are bubbles air in hydrogels).

3.6. Antimicrobial activity

The choice of 5-methoxysalicylaldehyde **(A)** as aldehyde for chitosan's hydrogelation took into consideration its natural origin which increases the probability of *in vivo* biocompatibility and also its potential antimicrobial activity demonstrated against some pathogens such as *Aspergillus flavus* [47,48] *Aspergillus fumigatus*, *A. terreus* and *Penicillium expansum* [49], *Mycobacterium avium* [50] and *Escherichia coli* [51].

In this regard, the antimicrobial activity of the hydrogels was investigated on relevant pathogens that play essential role in human health, such as gram positive (*S.aureus*), gram-negative (*E.coli*), yeast (*C. albicans* and *C. glabrata*) and fungal (*P. chrysogenum*, *C. cladosporioides*, *A. brasiliensis*) strains by agar disk diffusion method. For a proper comparison, chitosan and aldehyde precursors were investigated as controlso, at the same concentration as in hydrogels. The results were presented in Fig. 9 and Table S3.

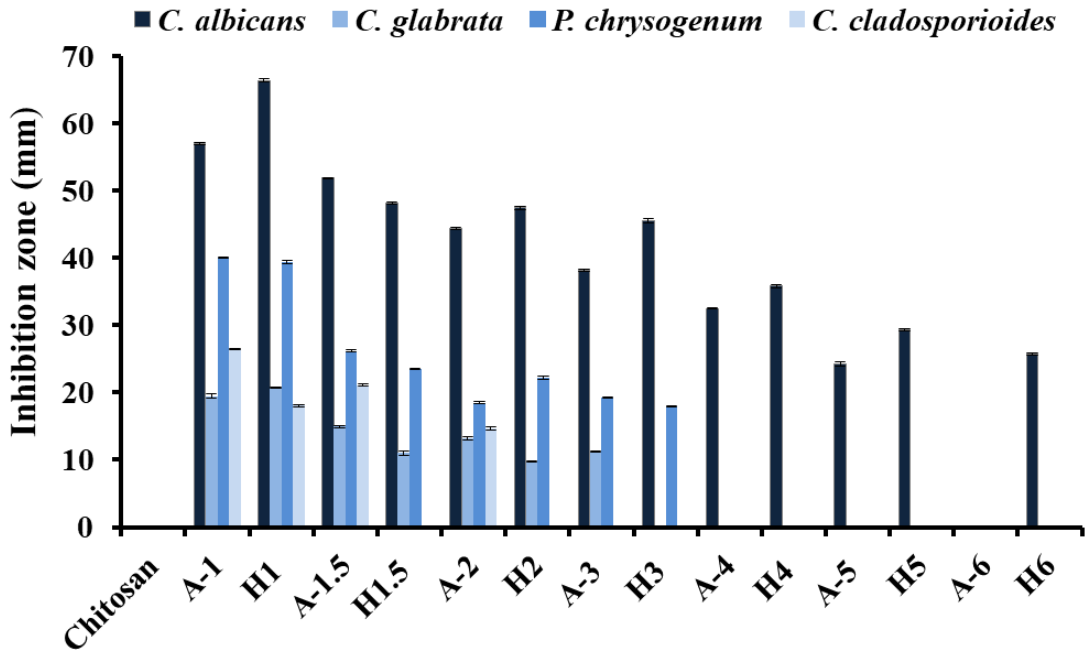

a)

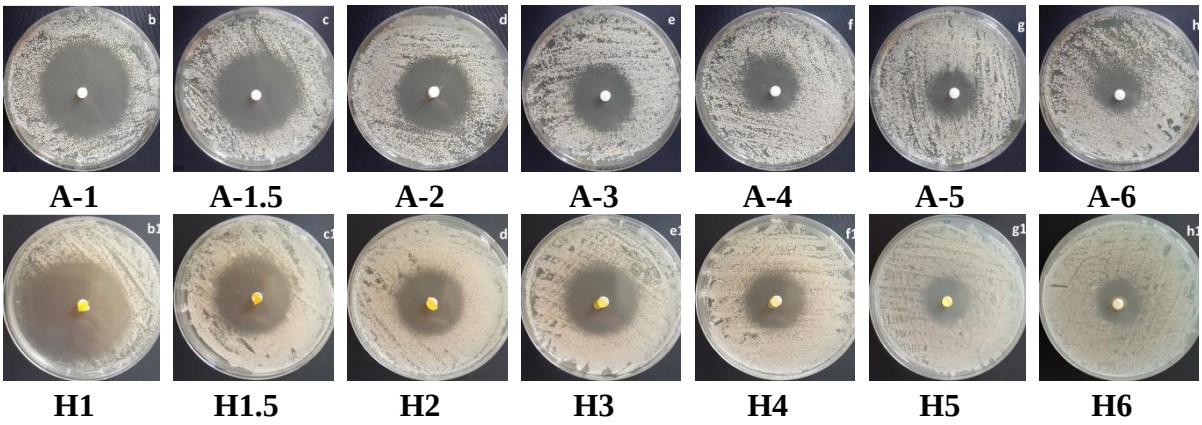

Fig. 9. a) Graphical representation of the inhibition zones on various fungal strains and b) representative images for the case of *C.albicans*

Contrary to the literature data, chitosan did not present any antimicrobial activity (see Table S3 and Fig. S5) [52-54]. The hydrogels and 5-methoxysalicylaldehyde (**A**) presented concentration dependent antifungal activity, the inhibition zone decreasing once the 5-methoxysalicylaldehyde concentration decreased (Fig. 9, Table S3). The highest activity was noticed against the *C. albicans*, reaching an inhibition zone of 66 mm in the case of hydrogel ***H1*** (Fig. 9). Interesting enough, the hydrogels were slightly more efficient against *C. albicans* compared with their aldehyde controls. High antifungal activity was also displayed against *P. chrysogenum* (around 40 mm), and good activity was recorded against *C. glabrata* (around 20 mm) and *C. cladosporioides* (around 20 mm), for the highest concentrations of the aldehyde and the corresponding hydrogels. In these cases, the antifungal activity of hydrogels did not exceed that of the aldehyde control, on contrary it was slightly lower. No inhibition zone was recorded against *S. aureus, E. coli* and *E. faecalis* for the hydrogels or corresponding aldehyde controls. From these data it appeared that the studied hydrogels have a specific affinity for *C. albicans* yeast, higher than their precursors. This is an intriguing finding, considering the aldehyde mobility in the two samples: (i) high mobility in solution assuring a very fast diffusion of the 5-methoxysalicylaldehyde molecules into the yeast medium, and (ii) low mobility in hydrogel state with 5-methoxysalicylaldehyde covalently bonded *via* imine linkage to the chitosan. It is possible as the reversible nature of imine linkage to play an important role in this behavior. It is expected that the reaction equilibrium to be shifted to the reagents once 5-methoxysalicylaldehyde is consumed in the process of *C. albicans* inhibition [4, 55]. This can lead to the release of the 5-methoxysalicylaldehyde in a controlled manner under the *C. albicans*

stimuli improving its bioavailability, compared to the free aldehyde in solution which easier can volatilize.

This hypothesis was supported by the investigation of 5-methoxysalicylaldehyde release in a medium mimicking the microbiologic environment (Fig.10). It was observed that the aldehyde was rapidly released during 4 hours, progressively in the next 4 days, reaching then a plateau in line with the establishing of the imination equilibrium. The amount of the released aldehyde over time increased as the crosslinking degree decreased, triggered by the lower concentration of the released aldehyde in the medium, which forced the imination shifting to the reagents.

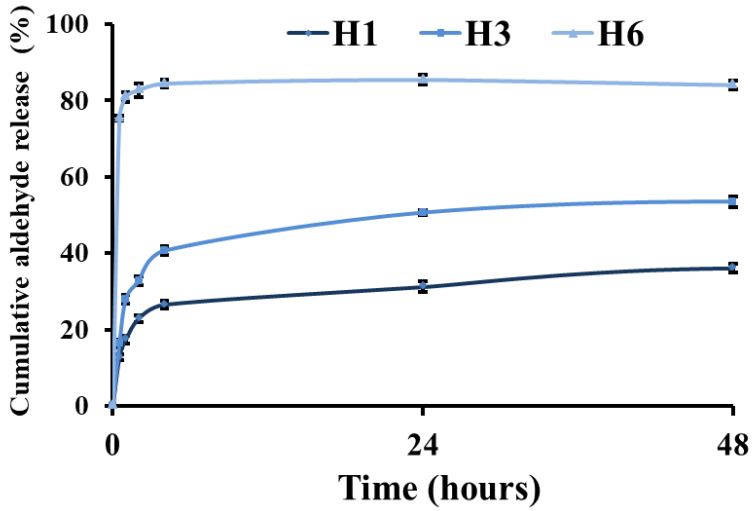

Fig.10. The aldehyde release over 48 hours, at 37ºC

3.7. Swelling and stability studies of 5-methoxysalicyl-imine-chitosan hydrogels (Hx)

Swelling and stability at different pHs are important characteristics of hydrogels which can determine their application, especially *in vivo* ones. In this light, the swelling ability and stability of the hydrogels were investigated at three different pHs: 7.4 which is the physiological pH; 5.5 – characteristic for normal dermis, and 8.5 characteristic for infected tissues [4, 56]. As the antimicrobial and biocompatibility tests indicated ***H1.5***, ***H2***, and ***H3*** samples as the most promising for wound healing, they were further investigated (Fig. 11 and Table S4, S5, S6).

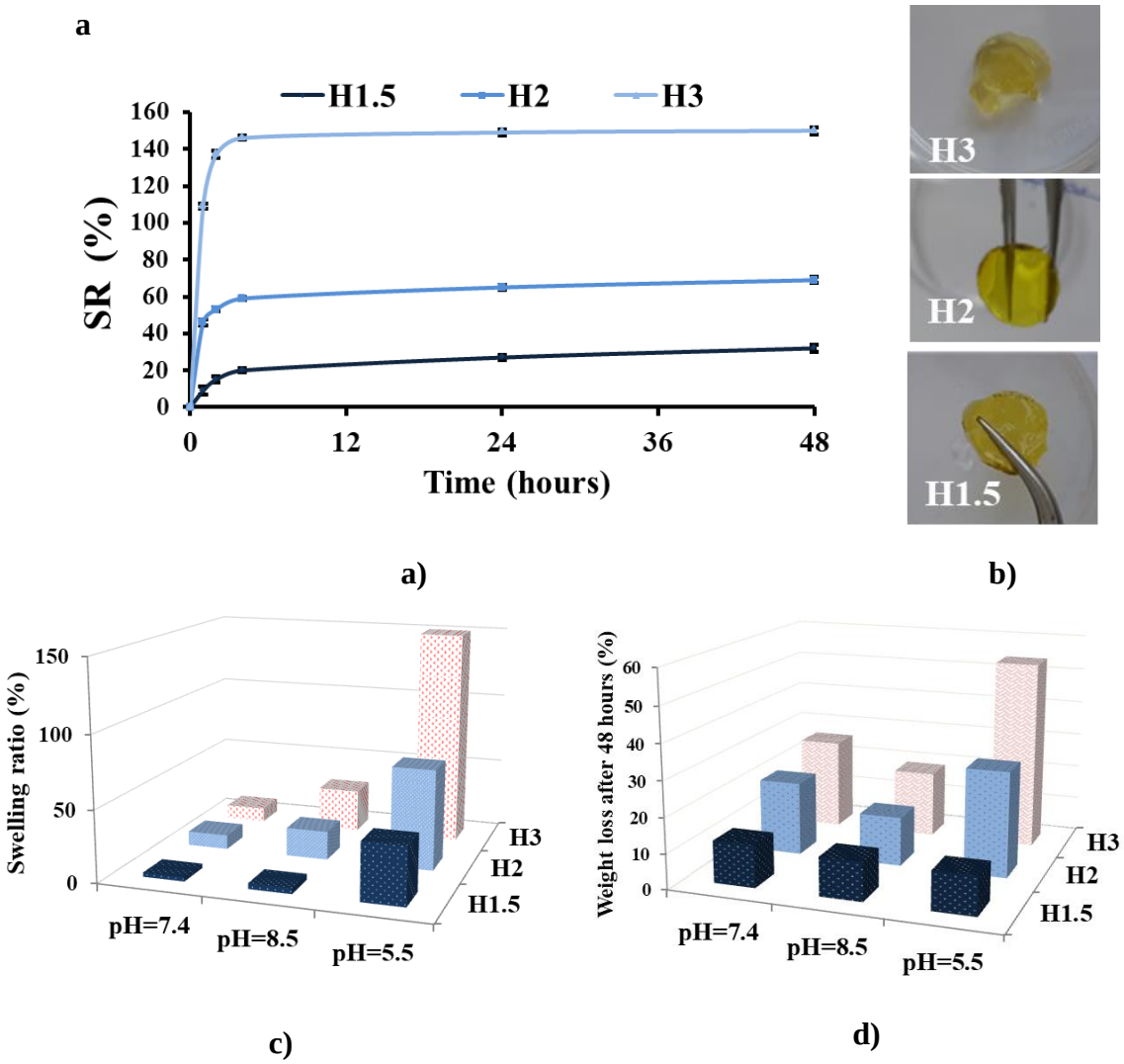

Fig. 11. The swelling and mass loss of hydrogels investigated in media of different pH, at 37 ^{o}C over 48 hours: a) swelling kinetics in PBS (pH=5.5); b) images of hydrogels after swelling in PBS (pH=5.5); c) the swelling ratio and d) the mass loss, in media of different pH

The hydrogels rapidly swelled in all media and reached the mass equilibrium within 30 minutes (Fig. 11c and Table S4). The swelling ratio increased once the crosslinking density of samples decreased, in line with their morphology; those with lower crosslinking density which presented a loose network of pores and fibers (***H2*** and ***H3***) allowed a higher swelling compared with those with higher crosslinking density which presented interconnected pores (***H1.5***). Comparing the hydrogels' behavior in different pH media, a higher swelling ratio was reached in acidic environment (Fig.11a, b and Table S5). This was explained by the high protonation of free NH_2 groups of chitosan in acidic medium, causing electrostatic repulsions amongst the positive charges and disruption of the H-bonds. Consequently, the network expanded and more water could diffuse into the hydrogel [57]. On the other hand, the higher mass loss at pH=5.5

indicated a greater dissolution due to the hydrolysis of the imine units, which impacted a much loss morphology and consequently an increased swelling (Fig. 11a and b). In media of physiological pH, a slight increase of the swelling ratio was noticed, with insignificant modification of the hydrogel shape. This behavior is in agreement with the deprotonating of free NH_2 groups in basic media, which favored the H-bond interactions and consequently reduced the swelling capacity [17]. Interesting enough, at more basic pH (8.5) the swelling ratio slightly increased.

Regarding the ***hydrogels' stability***, the sample weighting after 2 days showed a higher mass loss for the hydrogels with lower crosslinking degree and it was more advanced in acidic media (Fig. 11d and Table S6). All hydrogels were visual stable in the first 9 days of experiment, after that, the erosion of the ***H3*** was obvious, while the other samples were visual stable over 3 months of investigation.

3.8. Visual analysis of self-healing properties of the hydrogels

The hydrogelation mechanism of these hydrogels relies on the formation of reversible covalent imine linkages, which are favorable for a self-healing process [10, 20]. Therefore, this possibility was investigated. Firstly, the hydrogels were injectable through a syringe needle and their structure was able to recover after applying a mechanical force. Another approach was to use Rhodamine B to mark one hydrogel, and after that it was injected through a syringe needle on the unmarked hydrogel. It was observed that these two different injected hydrogels were able to connect forming a single piece (Fig. 12). Further, they were mechanical crushed and instantaneous after the mechanical force removing, they formed a single piece again [58]. This behavior points for an easy manipulation at applying on wounds.

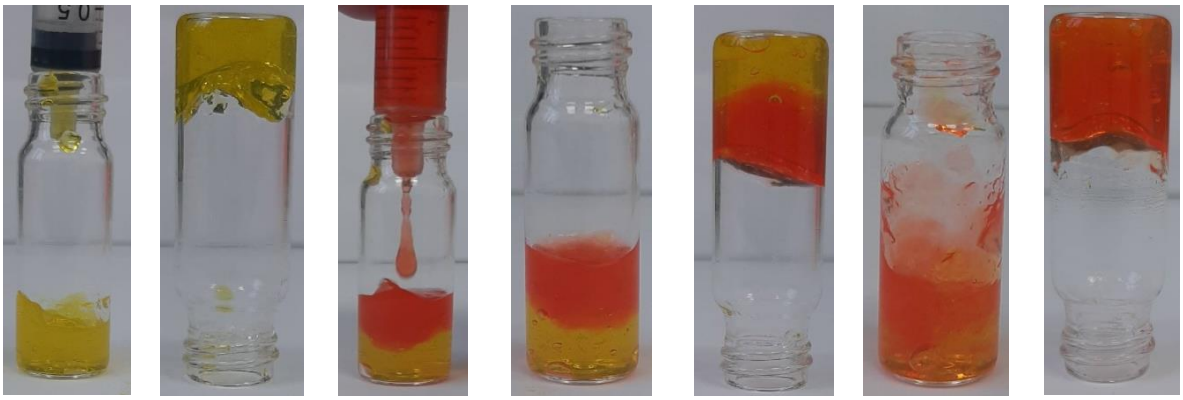

Fig. 12. Visual assessment of the self-healing ability of the hydrogels, exemplified on ***H3***

3.9. In vitro enzymatic biodegradation

The biodegradation behavior of the hydrogels was evaluated in terms of weight loss over a period of 21 days, in conditions mimicking the environment of infected wounds: lysozyme solution of pH 8.5 at 37°C (Fig. 13) [4]. The lysozyme was chosen due to its presence in wound fluid, and its ability to hydrolyze the chitosan into oligomers [59, 60].The most promising samples for *in vivo* applications were chosen for this study (Fig. 13).

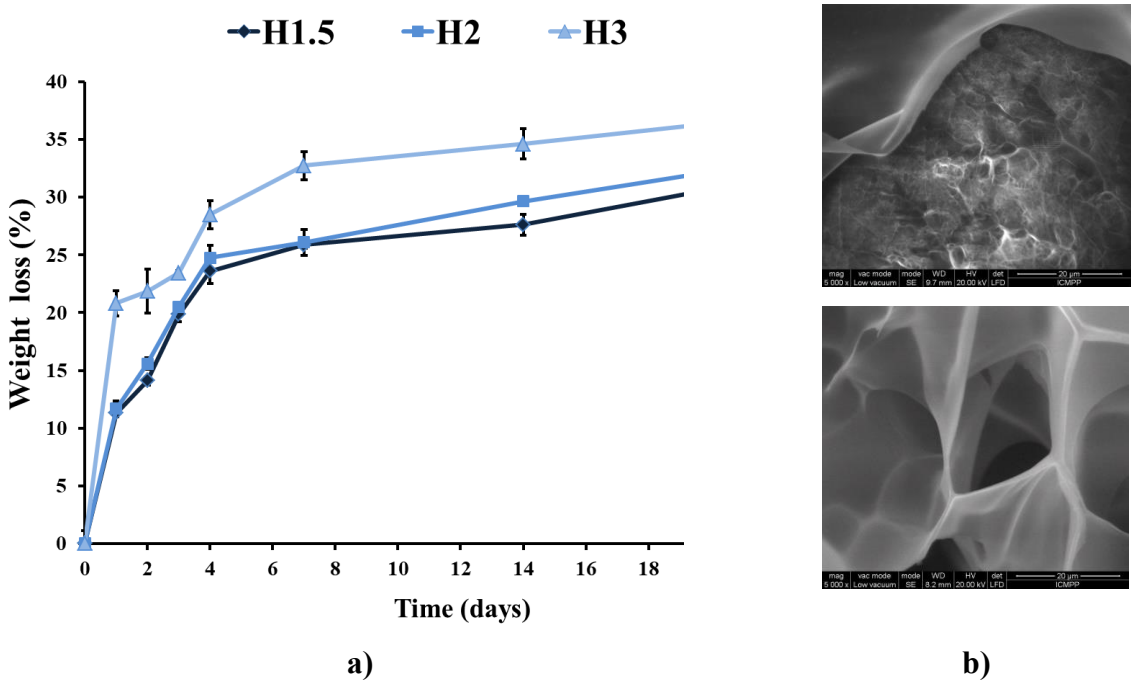

Fig.13. a) *In vitro* biodegradation profile of representative hydrogels over 21 days. Triplicates of all sample were evaluated (n = 3), and each point shows the mean value ± standard deviation; **b)** images of the hydrogels after degradation

As can be seen in Fig. 13a, the biodegradation occurred in three stages of different degradation rates. Thus, in the first day of investigation, an abrupt mass loss of 11% for ***H1.5*** and ***H2*** and 21% for ***H3*** was recorded (stage I). In the next 3 days, the biodegradation continued in a slower manner, reaching a mass loss around 24% for ***H1.5*** and ***H2*** and 29% for ***H3***, with an average degradation of 6.5 and 3% per day (stage II). Further, in the next 17 days, the rate of mass loss slowed down more at around 0.75% per day, reaching a total mass loss of 31% for ***H1.5*** and ***H2*** and 37% for ***H3*** (stage III). The massive mass loss in the first stage was correlated with the cleavage of the O-C bonds between consecutive N-acetyl-D-glucosamine units catalyzed by lysozyme, leading to chitosan oligomers and their diffusion to the media. The higher biodegradation rate of ***H3*** was attributed to its more porous structure which facilitated the absorption of water and lysozyme into the hydrogel network structure, as its swelling

behavior in PBS indicated (swelling rate of 30%, compared to 10% and 4%). Further, in the second biodegradation stage, it is expected as the cleavage of the O-C bonds catalyzed by lysozyme to continue, especially for the ***H1.5*** and ***H2*** samples with slower swelling in basic pH. The higher mass loss of ***H3*** compared to ***H1.5*** and ***H2*** can be also attributed to the hydrolysis of the reversible imine units. This favored the breaking of the crosslinking nodes, weakening the network and thus facilitating the lysozymes to access faster the proper sites. The slow release in the stage III, could be also affected by the mass loss observed in the swelling investigation. Combining the data from swelling and enzymatic degradation, it can be concluded that the biodegradation of this hydrogels was a result of the lysozyme effect (leading to the cleavage of the O-C bonds) and the erosion by dissolution of the chitosan [60]. The visualization of the hydrogels after degradation showed smaller pores (Figure 13b) indicating a reorganization of the hydrogel during biodegradation, possible due to the formation of new imine units by imination and transamination reactions [38], as the self-healing behavior indicated.

3.10. Conclusions

New natural originating hydrogels with good biocompatibility and antifungal properties were prepared by a simple and easy method from chitosan and a vanillin isomer, i.e. 5-methoxysalicylaldehyde. It was demonstrated that the driving force of hydrogelation rely on the forming of covalent reversible imine bonds and supramolecular organization of the new formed imine units in clusters playing the role of crosslinking nodes. An optimal amount of aldehyde used for chitosan crosslinking generated hydrogels with suitable biocompatibility for medical devices and remarkable antifungal activity. These hydrogels presented porous morphology and consequently good swelling in media mimicking different biologic fluids (e.g. physiological pH, pH of infected tissues and pH of normal dermis) pointing for a good oxygen permeation and exudate drainage. Besides, they were biodegradable and presented self-healing behavior indicating easy manipulation in view of application on skin lesions.

Acknowledgements

The research leading to these results has received funding from the Romanian National Authority for Scientific Research, MEN-UEFISCDI grant, project number RO-NO-2019-0540 (14/2020).

References

[1] X. Zhao, H. Wu, B. Guo, R. Dong, Y. Qiu, P.X. Ma. Antibacterial anti-oxidant electroactive injectable hydrogel as self-healing wound dressing with hemostasis and adhesiveness for cutaneous wound healing, *Biomaterials* 122 (2017) 34–47. https://doi.org/10.1016/j.biomaterials.2017.01.011.

[2] M.A. Matica, F.L. Aachmann, A. Tøndervik, H. Sletta, V. Ostafe. Chitosan as a wound dressing starting material: Antimicrobial properties and mode of action. *Int. J. Mol. Sci.* 20 (2019), 5889. https://doi.org/10.3390/ijms20235889.

[3] P. Hubner, N. Donati, L. Kelin, D.M. Quines, I.C. Tessaro, N.R. Marcilio**.** Gelatin-based films containing clinoptilolite-Ag for application as wound dressing. *Mater. Sci. Eng. C.* 107 (2020) 110215. https://doi.org/10.1016/j.msec.2019.110215.

[4] A. Anisiei, I. Rosca, A.I. Sandu, A. Bele, X. Cheng, L. Marin, Imination of Microporous Chitosan Fibers—A Route to Biomaterials with "On Demand" Antimicrobial Activity and Biodegradation for Wound Dressings, *Pharmaceutics* 14 (2022) 117; https://doi.org/10.3390/pharmaceutics14010117.

[5] J. Su, J. Li, J. Liang, K. Zhang, J. Li. Hydrogel preparation methods and biomaterials for wound dressing. *Life* 11 (2021) 1016. https://doi.org/10.3390/life11101016.

[6] Z. Hussain, H.E. Thu, A.N. Shuid, H. Katas, F. Hussain, Recent advances in polymer-based wound dressings for the treatment of diabetic foot ulcer: An overview of state-of-the-art, *Curr. Drug Targets* 19 (2018) 527–550. https://doi.org/10.2174/1389450118666170704132523.

[7] A. Zhang, Y. Liu, D. Qin, M. Sun, T. Wang, X. Chen, Research status of self-healing hydrogel for wound management: A review, *Int. J. Biol. Macromol*. 164 (2020) 2108–2123. https://doi.org/10.1016/j.ijbiomac.2020.08.

[8] S.P. Ndlovu, K. Ngece, S. Alven, B.A. Aderibigbe. Gelatin-Based Hybrid Scaffolds: Promising Wound Dressings. *Polymers* 13 (2021) 2959. https://doi.org/10.3390/polym13172959.

[9] J. Jagur-Grodzinski, Polymeric gels and hydrogels for biomedical and pharmaceutical applications, *Polym. Adv. Technol.* 21 (2011) 27–47. https://doi.org/10.1002/pat.1504.

[10] Z. Li, Y. Huang, R. Yu, B. Guo, Dual-dynamic-bond cross-linked antibacterial adhesive hydrogel sealants with on-demand removability for post-wound-closure and infected wound healing, *ACS Nano* 15 (2021) 7078–7093. https://doi.org/10.1021/acsnano.1c04206.

[11] T. Dai, M. Tanaka, Y. Huang, M. Hamblin, Chitosan preparations for wounds and burns: Antimicrobial and wound-healing effects, *Expert. Rev. Anti. Infect. Ther*. 9 (2011) 857–879. https://doi.org/10.1586/eri.11.59.

[12] J. Flynn, E. Durack, M. N. Collins, S. P. Hudson, Tuning the strength and swelling of an injectable polysaccharide hydrogel and the subsequent release of a broad spectrum bacteriocin, nisin A, *J. Mater. Chem. B.* 8 (2020) 4029–4038, https://doi.org/10.1039/d0tb00169d.

[13] B.I. Andreica, D. Ailincai, A.I. Sandu, L. Marin, Amphiphilic chitosan-g-poly(trimethylene carbonate) - A new approach for biomaterials design, *Int J Biol Macromol.* 193 (2021) 414–424. https://doi.org/10.1016/j.ijbiomac.2021.10.174.

[14] S. Li, S. Dong, W. Xu, S. Tu, L.Yan, C. Zhao, J. Ding, X. Chen, Antibacterial hydrogels. *Adv. Sci*. 5 (2018) 1700527. https://doi.org/10.1002/advs.201700527.

[15] M. Li, Y. Liang, J. He, H. Zhang, B. Guo, Two-pronged strategy of biomechanically active and biochemically multifunctional hydrogel wound dressing to accelerate wound closure and wound healing, *Chem. Mater*. 32 (2020) 9937–9953. https://dx.doi.org/10.1021/acs.chemmater.0c02823.

[16] Z. Yang, S. Hideyoshi, H. Jiang, Y. Matsumura, J.L. Dziki, S.T. Lopresti, L. Huleihel, G.N.F. Faria, L.C. Fuhrman, R. Lodono. Injectable, porous, biohybrid hydrogels incorporating decellularized tissue components for soft tissue applications. *Acta Biomaterialia* 73 (2018) S1742706118301934. https://doi.org/10.1016/j.actbio.2018.04.003.

[17] R. Rakhshaei, H. Namazi, A potential bioactive wound dressing based on carboxymethyl cellulose/ZnO impregnated MCM-41 nanocomposite hydrogel, *Mater. Sci. Eng. C Mater. Biol.* 73 (2017) 456–464. https://doi.org/10.1016/j.msec.2016.12.097.

[18] X. Qu, A. Wirsen, A.-C. Albertsson, Novel pH-sensitive chitosan hydrogels: swelling behavior and states of water, *Polymer* 41 (2000) 4589–4598. https://doi.org/10.1016/S0032-3861(99)00685-0.

[19] E.A. Kamoun, E.R. Kenawy, X. Chen, A review on polymeric hydrogel membranes for wound dressing applications: PVA-based hydrogel dressings, *J. Adv. Res*. 8 (2017) 217–233. https://doi.org/10.1016/j.jare.2017.01.005.

[20] M.M. Iftime, S. Morariu, L. Marin, Salicyl-imine-chitosan hydrogels: Supramolecular architecturing as a crosslinking method toward multifunctional hydrogels, *Carbohydr. Polym*. 165 (2017) 39–50. https://doi.org/10.1016/j.carbpol.2017.02.027.

[21] L. Marin, D. Ailincai, S. Morariu, L. Tartau-Mititelu, Development of biocompatible glycodynameric hydrogels joining two natural motifs by dynamic constitutional chemistry, *Carbohydr. Polym*. 170 (2017), 60–71. https://doi.org/10.1016/j.carbpol.2017.04.055.

[22] A.M. Olaru, L. Marin, S. Morariu, G. Pricope, M. Pinteala, L. Tartau-Mititelu, Biocompatible based hydrogels for potential application in local tumour therapy, *Carbohydr. Polym*. 179 (2018) 59–70. https://doi.org/10.1016/j.carbpol.2017.09.066.

[23] D. Ailincai, L. Marin, S. Morariu, M. Mares, A.C. Bostanaru, M. Pinteala, B.C.Simionescu, M. Barboiu, Dual crosslinked iminoboronate-chitosan hydrogels with strong antifungal activity against *Candida planktonic* yeasts and biofilms, *Carbohydr. Polym.* 152 (2016) 306–316. https://doi.org/10.1016/j.carbpol.2016.07.007.

[24] M. Iftime, L. Marin, Chiral betulin-imino-chitosan hydrogels by dynamic covalent sonochemistry, *Ultrason. Sonochem*. 45 (2018) 238–247. https://doi.org/10.1016/j.ultsonch.2018.03.022.

[25] L. Marin, S. Moraru, M.C. Popescu, A. Nicolescu, C. Zgardan, B.C. Simionescu, M. Barboiu, Out-of-Water Constitutional Self-Organization of Chitosan-Cinnamaldehyde Dynagels, Chem. Eur. J. 20 (2014) 4814–4821. https://doi.org/10.1002/chem.201304714.

[26] A. Bejan, F. Doroftei, X. Cheng, L. Marin, Phenothiazine-chitosan based eco-adsorbents: A special design for mercury removal and fast naked eye detection, *Int J Biol Macromol.*162 (2020) 1839–1848. https://doi.org/10.1016/j.ijbiomac.2020.07.232

[27] C.W. Li, L. Marin, X.J. Cheng, Chitosan based macromolecular probes for the selective detection and removal of Fe^{3+} ion, *Int. J. Biol. Macromol*. 186 (2021) 303–313. https://doi.org/10.1016/j.ijbiomac.2021.07.044.

[28] A.R. Kumar, V. Nithya, S. Rajeshkumar, S. Gunasekaran et al., An experimental and theoretical evidence for structural and spectroscopic properties of 2-hydroxy-5-methoxybenzaldehyde, *The International Journal of Analytical and Experimental Modal Analysis*. XI (2019)1990-2003. ISSN NO: 0886-9367.

[29] M.M. Iftime, L. Mititelu Tartau, L. Marin, New formulations based on salicyl-imine-chitosan hydrogels for prolonged drug release, *Int. J. Biol. Macromol*. 160 (2020) 398–408. https://doi.org/10.1016/j.ijbiomac.2020.05.207.

[30] X. Wang, P. Xu, Z. Yao, Q. Fang, L. Feng, R. Guo, B. Cheng, Preparation of antimicrobial hyaluronic acid/quaternized chitosan hydrogels for the promotion of seawater-immersion wound healing. *Front. Bioeng. Biotechnol*. 7 (2019) 360. https://doi.org/10.3389/fbioe.2019.00360.

[31] N.A. Mohamed, N.A. Abd El-Ghany, M.M. Abdel-Aziz, Synthesis, characterization, anti-inflammatory and anti-Helicobacter pylori activities of novel benzophenone tetracarboxylimide benzoyl thiourea cross-linked chitosan hydrogels, *Int. J. Biol. Macromol*. 181 (2021) 956–965. https://doi.org/10.1016/j.ijbiomac.2021.04.095.

[32] A.R. Karimi, B. Rostaminejad, L. Rahimi, A. Khodadadi, H. Khanmohammadi, A. Shahriari, Chitosan hydrogels cross-linked with tris(2-(2-formylphenoxy)ethyl) amine: Swelling and drug delivery, *Int. J. Biol. Macromol*. 118 (2018) 1863–1870. https://doi.org/10.1016/j.ijbiomac.2018.07.037.

[33] A.M. Craciun, L. Mititelu-Tartau, G. Gavril, L. Marin. Chitosan crosslinking with pyridoxal 5-phosphate vitamer toward biocompatible hydrogels for *in vivo* applications, *Int. J. Biol. Macromol*. (2021) https://doi.org/10.1016/j.ijbiomac.2021.10.22.

[34] ISO 10993-5:2009 Biological evaluation of medical devices. Part 5: Tests for *in vitro* cytotoxicity. *International Organization for Standardization*, Geneva, Switzerland, 2009.

[35] M. Yildirim-Aksoy, B.H. Beck, Antimicrobial activity of chitosan and a chitosan oligomer against bacterial pathogens of warm water fish, *J. Appl. Microbiol*. 122 (2017) 1570–1578. https://doi.org/10.1111/jam.13460.

[36] Statistical analysis was performed XLSTAT software, Addinsoft, 2021. XLSTAT statistical and data analysis solution. New York, USA. https://www.xlstat.com.

[37] S. Bratskaya, Y. Privar, A. Skatova, A. Slobodyuk, E. Kantemirova, A. Pestov, Carboxyalkylchitosan-based hydrogels with “imine clip”: Enhanced stability and amino acids-induced disassembly under physiological conditions. *Carbohydr. Polym*. 274, (2021) 118618. https://doi.org/10.1016/j.carbpol.2021.118618.

[38] P. Kovaricek, J.M. Lehn, Merging constitutional and motional covalent dynamics in reversible imine formation and exchange processes, *J. Am. Chem. Soc*. 134 (2012) 9446–9455. https://doi.org/10.1021/ja302793c.

[39] A. Anisiei, A.C. Bostanaru, M. Mares, L. Marin, Imination of chitosan nanofibers in a heterogeneous system. Synthesis optimization and impact on fiber morphology, Cell. Chem. Technol. 55 (2021), 785–793. https://doi.org/10.35812/CelluloseChemTechnol.2021.55.65.

[40] A.M. Craciun, L. Mititelu Tartau, M. Pinteala, et al., Nitrosalicyl-imine-chitosan hydrogels based drug delivery systems for long term sustained release in local therapy, *J. Colloid Interface Sci*. 536 (2019) 196–207. https://doi.org/10.1016/j.jcis.2018.10.048.

[41] P.D. Chatterjee, M. Pakhira, A.K. Nandi, Fluorescence in “nonfluorescent” polymers, *ACS Omega.* 5 (2020) 30747–30766. https://doi.org/10.1021/acsomega.0c04700.

[42] M. Barón, Definitions of basic terms relating to low-molar-mass and polymer liquid crystals, *Pure Appl. Chem*. 73 (2001) 845–895. http://dx.doi.org/10.1351/pac200173050845.

[43] Estrela dos Santos, E.R. Dockal, É.T.G. Cavalheiro, Thermal behavior of Schiff bases from chitosan, *J. Therm. Anal. Cal*., 79 (2005) 243–248. https://doi.org/10.1007/s10973-005-0042-x.

[44] C.G.T. Netoa, J.A. Giacomettib, A.E. Jobb, F.C. Ferreirab, J.L.C. Fonsecaa, M.R. Pereira, Thermal analysis of chitosan based networks, *Carbohydr. Polym.* 62 (2005) 97–103.

[45] Y. Liang, Z. Li, Y. Huang, R. Yu, B. Guo, Dual-dynamic-bond cross-linked antibacterial adhesive hydrogel sealants with on-demand removability for post-wound- closure and infected wound healing, *ACS Nano* 15 (2021) 7078−7093. https://doi.org/10.1021/acsnano.1c00204.

[46] O.O. Ige, L.E. Umoru, S. Aribo, 2012. Natural products: A minefield of biomaterials. *Int. Sch. Res. Notices*, 983062. https://doi.org/10.5402/2012/983062.

[47] Q. Li, X. Zhu, Vanillin and its derivatives, potential promising antifungal agents, inhibit *Aspergillus flavus* spores via destroying the integrity of cell membrane rather than cell wall, *GOST*, 4 (2021) 54–61. https://doi.org/10.1016/j.gaost.2021.03.002.

[48] E.Y. Jeong, M.Ji Lee, M.S. Kang, H.S. Lee, Antimicrobial agents of 4-methoxysalicylaldehyde isolated from Periploca sepium oil against foodborne bacteria: structure–activity relationship, *Appl. Biol. Chem*. 61 (2018) 397–402. https://doi.org/10.1007/s13765-018-0373-5.

[49] J.H. Kim, K.L. Chan, N. Mahoney, B.C. Campbell, 2011. Antifungal activity of redox-active benzaldehydes that target cellular antioxidation. *Ann. Clin. Microbiol. Antimicrob*. 10, 23. https://doi.org/10.1186/1476-0711-10-23.

[50] S.Y.Y. Wong, I. R. Grant, M. Friedman, C.T. Elliott, C. Situ, Antibacterial activities of naturally occurring compounds against *Mycobacterium avium subsp. paratuberculosis*, *Appl. Environ. Microbiol*. (2008) 5986–5990. https://doi.org/10.1128/AEM.00981-08.

[51] M. Friedman, P.R. Henika, R.E. Mandrell, Antibacterial activities of phenolic benzaldehydes and benzoic acids against *Campylobacter jejuni*, *Escherichia coli*, *Listeria monocytogenes*, and *Salmonella enterica*, *J. Food Prot*. 66 (2003) 10 1811–1821. https://doi.org/10.4315/0362-028X-66.10.1811.

[52] S.P. Chen, G.Z. Wu, D.W. Long, Y.D. Liu, Preparation, characterization and antibacterial activity of chitosan-Ca3V10O28 complex membrane, *Carbohydr. Polym*. 64 (2006) 92–97. https://doi.org/10.1016/j.carbpol.2005.10.024.

[53] R.C. Goy, D. Britto, O.B.G. Assis, A review of the antimicrobial activity of chitosan, *Polímeros* 19 (2009) 241–247. https://doi.org/10.1590/S0104-14282009000300013.

[54] Z. Guo, R. Chen, R. Xing, S. Liu, H. Yu, P. Wang, C. Li, P. Li, Novel derivatives of chitosan and their antifungal activities *in vitro*, *Carbohydr. Res*. 341 (2006) 351–354. https://doi.org/10.1016/j.carres.2005.11.002S.

[55] L. Marin, M. Popa, A. Anisiei, S.A. Irimiciuc, M. Agop, T.C. Petrescu, D. Vasincu, L. Himiniuc, A Theoretical Model for Release Dynamics of an Antifungal Agent Covalently Bonded to the Chitosan, *Molecules* 26 (2021) 2089. https://doi.org/10.3390/molecules26072089.

[56] E. Osti, Skin pH variations from the acute phase to re-epithelialization in burn patients treated with new materials (Burnshield®, semipermeable adhesive film, Dermasilk®, and Hyalomatrix®). Non-invasive preliminary experimental clinical trial, *Ann. Burns Fire Disasters* 21 (2008) 73–77.

[57] G.M.D. Salah Uddin, S. Saha, S. Karmaker, T. Kumar Saha, Adsorption of cefixime trihydrate onto chitosan 10b from aqueous solution: kinetic, equilibrium and thermodynamic studies, *Cellulose Chem. Technol*. 55 (2021) 771-784. https://doi.org/10.35812/CelluloseChemTechnol.2021.55.64.

[58] D. Ailincai, I. Rosca, S. Morariu, L. Mititelu-Tartau, L. Marin. Iminoboronate-chitooligosaccharides hydrogels with strong antimicrobial activity for biomedical applications. *Carbohydr. Polym*. 276 (2022) 118727. https://doi.org/10.1016/j.carbpol.2021.118727.

[59] D.E. Kuehner, J. Engmann, F. Fergg, M. Wernick, H.W. Blanch, J.M. Prausnitz, Lysozyme net charge and ion binding in concentrated aqueous electrolyte solutions, *J. Phys. Chem. B*. 103 (1999) 1368–1374.

[60] S. Hirano, H. Tsuchida, N. Nagao, N-acetylation in chitosan and the rate of its enzymic hydrolysis, *Biomaterials*. 10 (1989) 574–576. https://doi.org/10.1016/0142-9612(89)90066-5.

Graphical Abstract